

Canonical Motor Microcircuit for Control of a Rat Hindlimb

Clayton Jackson^{1(\boxtimes)}, William R. P. Nourse², C. J. Heckman³, Matthew Tresch⁴, and Roger D. Quinn¹

- Department of Mechanical and Aerospace Engineering, Case Western Reserve University, Cleveland, OH 44106-7222, USA clayton.jackson@case.edu
- ² Department of Electrical, Computer, and Systems Engineering, Case Western Reserve University, Cleveland, OH 44106-7222, USA
 - ³ Department of Physical Therapy and Human Movement Sciences, Northwestern University, Evanston, IL 60208, USA
 - Department of Biomedical Engineering, Northwestern University, Evanston, IL 60208, USA

Abstract. This work focuses on creating a controller for the hip joint of a rat using a canonical motor microcircuit. It is thought that this circuit acts to modulate motor neuron activity at the output stage. We first created a simplified biomechanical model of a rat hindlimb along with a neural model of the circuit in a software tool called Animatlab. The canonical motor microcircuit controller was then tuned such that the trajectory of the hip joint was similar to that of a rat during locomotion. This work describes a successful method for hand-tuning the various synaptic parameters and the influence of Ia feedback on motor neuron activity. The neuromechanical model will allow for further analysis of the circuit, specifically, the function and significance of Ia feedback and Renshaw cells.

Keywords: Canonical Motor Microcircuit \cdot Renshaw cells \cdot Neuromechanical simulation \cdot Rat

1 Introduction

The neural circuit used for locomotion in mammals continues to be a topic of research. A prevailing theory is that central pattern generators (CPG's) drive the motor neurons to produce the repetitive, rhythmic joint motion for walking [11]. In addition to these CPG's, there are a variety of lower-level circuits which act to modulate motor neuron activity and include muscle feedback. An example of one of these was introduced by Hultborn et al. [5]. We have created a model which we call the Canonical Motor Microcircuit (CMM), which loosely resembles the Hultborn circuit but does not include gamma motoneurons for the sake of

This work was supported by NSF DBI 2015317 as part of the NSF/CIHR/DFG/FRQ/UKRI-MRC Next Generation Networks for Neuroscience Program.

[©] The Author(s), under exclusive license to Springer Nature Switzerland AG 2022 A. Hunt et al. (Eds.): Living Machines 2022, LNAI 13548, pp. 309–320, 2022. https://doi.org/10.1007/978-3-031-20470-8_31

simplicity [5]. The CMM is present in numerous models for mammalian locomotion but is typically driven by a CPG [8,12,16]. The current model of the CMM is meant to be a starting point, additional pathways will be added as the model expands. While the exact role of the CMM is unknown, it is replicated along the spinal cord and is thought to play a role in muscle control during locomotion. This circuit contains three types of neurons: alpha motor neurons, Ia inhibitory neurons, and Renshaw Cells and relies strongly on Ia feedback from the muscle spindles.

A study was conducted to examine the activity of a CMM in cats during fictive locomotion, showing that each of these three types of neurons are active during locomotion [14]. In addition, this study showed that the activity and timing of the Ia inhibitory neurons and Renshaw cells is directly tied to the alpha motor neurons. Although experiments such as these have been done to examine the CMM in animals, the function of this circuit, specifically the Renshaw cells, remains unclear. Due to the topology of the circuit, it can be seen that the Renshaw cells act to suppress excessive output from the motor neurons. Other theories include that the recurrent circuitry of the Renshaw cells acts as a variable gain regulator for the motor neurons [5]. However, the existence of some of these synaptic connections is controversial in itself.

2 Methods

2.1 Modeling

In order to examine the functionality of the CMM as well as the Renshaw cells and their connectivity, we created a model of a rat hindlimb and tuned a CMM to control a pair of flexor-extensor muscles for the hip joint. The hip joint was chosen as a starting point for this work, as the knee and ankle positions during walking are dependent on the position of the hip. Figure 1 shows a simplified model of a rat hindlimb created in Animatlab, which was adapted from Deng et al. [3,4]. The biomechanical model was simplified to only the pelvis, femurs, shins, feet and flexor-extensor muscle pairs modeled with a linear-Hill muscle model. Other models exist in the full musculoskeletal complexity of the rat hindlimb, this is a reduced biomechanical model used to evaluate the CMM [2,17]. For these experiments, the pelvis was fixed in place and the model performed air stepping.

The joint and muscle placement was modeled using data on rat hindlimbs [4, 7,10]. Figure 2 shows the CMM created in Animatlab which controls the muscles for one of the hip joints of the biomechanical model. The model shown in Fig. 2 was constructed using non-spiking leaky-integrator neural models:

$$C\frac{dV}{dt} = I_{app} - I_{leak} + \sum_{i=1}^{n} I_{syn_i}$$
 (1)

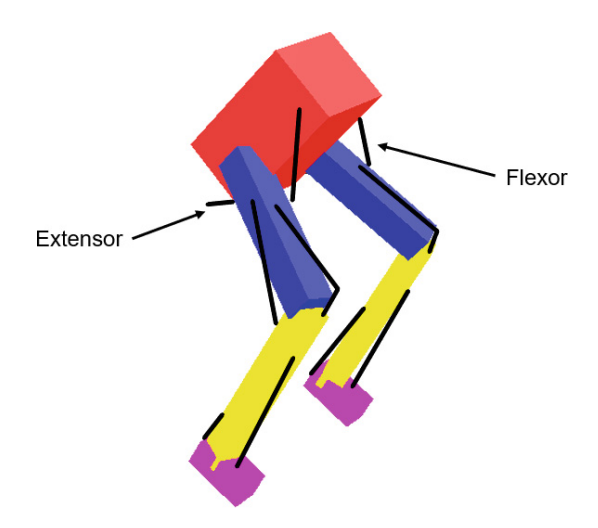


Fig. 1. Animatlab Biomechanical Model. Red: pelvis. Blue: femurs. Yellow: Shins. Pink: Feet. Black: Flexor and Extensor muscles. The flexor muscle pulls the leg forward while the extensor muscle pulls the leg backward. (Color figure online)

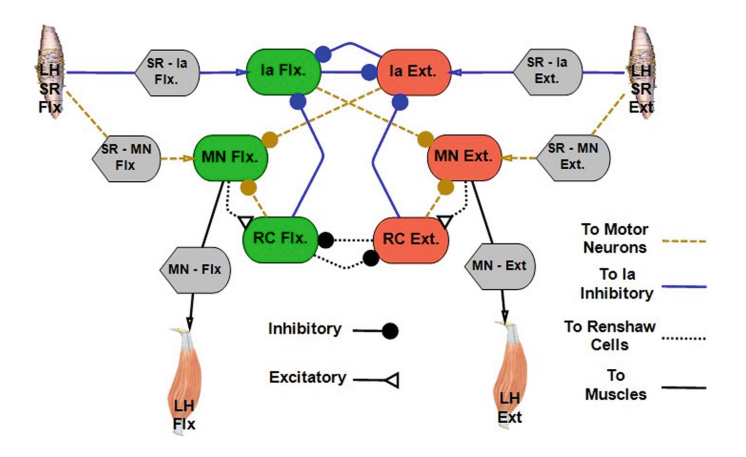


Fig. 2. CMM Neural Model in Animatlab. Ia: Ia inhibitory neuron. MN: alpha motor neuron. RC: Renshaw cell. LH: Left Hip. SR: stretch receptors for Ia type feedback. Grey Blocks: first order polynomial gains. (Color figure online)

where C is the membrane capacitance, V is the membrane voltage, I_{app} is an external applied current, I_{leak} is the membrane leak current, and I_{syn} are the synaptic currents. The inputs from the muscle stretch receptors were modeled as applied currents amplified by their respective gains, as implemented in Animatlab [3]:

$$I_{app_i} = S_i m_i + b_i \tag{2}$$

where S_i is the discharge rate of the stretch receptor, and m_i and b_i are slope and intercept of polynomial curve which amplifies the signal. Note that based on the values for these parameters as shown in Table 2, the neurons receive tonic input from the stretch receptors. The tonic input a function of both the resting discharge rate of the stretch receptor and the corresponding parameters in Table 2. The discharge rate of the stretch receptor is given by the equation [3]:

$$S_i = a(x - x_1) = \frac{aT}{K_{SE}} \tag{3}$$

where a is the active tension applied by stimulation of the membrane potential, x is the length of the muscle, x_1 is the length of the serial spring in the muscle, T is the muscle tension, and K_{SE} is the serial spring constants. The muscle tension is given by the differential equation [15]:

$$\dot{T} = \frac{K_{SE}}{b} \left(K_{PE} \Delta x(t) + b\dot{x}(t) - \left(1 + \frac{K_{PE}}{K_{SE}} \right) T(t) + a \right) \tag{4}$$

where K_{SE} is the stiffness of the serial elastic component, K_{PE} is the stiffness of the parallel elastic component, b is the linear damping coefficient, Δx is the change in muscle length relative to its resting length, and \dot{x} is the rate of change of the length off the muscle. The muscle properties used in the model were taken from Hunt et al. [7]. Further explanation for the muscle model can be found in Rubeo et al. [15]. The leak current in this generalized equation aims to model the net effect of sodium, potassium, and chloride channels with a net membrane conductance G and reversal potential E_R :

$$I_{leak} = G \cdot (V(t) - E_R). \tag{5}$$

Synaptic currents can be modeled as:

$$I_{syn_i} = G_{syn_i} \cdot (E_{syn_i} - V(t)) \tag{6}$$

where E_{syn} is the synaptic reversal potential, and G_{syn} is the synaptic conductance. The synaptic conductance is a function of the maximum conductance, g_{max_i} , the membrane potential of the pre-synaptic neuron, V_{pre} , and saturation and threshold parameters, E_{hi_i} and E_{lo_i} , which are properties of the pre-synaptic neuron:

$$G_{syn_i} = g_{max_i} \cdot \min\left(\max\left(\frac{V_{pre} - E_{lo_i}}{E_{hi_i} - E_{lo_i}}, 0\right), 1\right). \tag{7}$$

The advantage of using the non-spiking leaky-integrator model is that each neuron models the average activity of a population of spiking neurons [19]. These generalized equations were applied to each of the neurons in the CMM. For example, the equation for the motor neuron controlling the flexor muscle included a leak current term, an applied current modeling the input from the stretch receptor, and two synaptic current terms. This can be visualized by looking at the gold dashed lines attached to the flexor motor neuron in Fig. 2.

2.2 Tuning

The goal was to tune the parameters in the CMM such that the simulated hip angle resembles that of a rat walking. We used rat walking data to compare the outputs of the Animatlab simulation. This data for the hip trajectory of a rat walking on a treadmill was collected as described in Alessandro et al. and is not the focus of this work [1]. We predicted that the CMM network could be tuned to generate muscle activity for the hip joint of the rat hindlimb biomechanical model such that the angle of the hip joint in the simulation approximates that of a rat walking. We were confident in our ability to do so because of the abundance of inhibition in the network, which loosely resembles an oscillator. After successfully tuning the model, we then evaluated the relative strengths of the synaptic conductance's, specifically, the reciprocal inhibition between Renshaw cells.

We used two methods to tune the CMM. The first was done in a qualitative manner and aimed to produce oscillations in the network. The second method was a more quantitative approach, evaluating the oscillations in terms of a cost function comparing the simulated data to the animal data. There are a total of 72 parameters to tune in this network. These include synaptic properties, neural properties, and gain factors to and from muscles. We reduced the number of parameters by applying symmetry to the model. For example, on both the flexor and extensor side of the CMM there is a synapse going from the motor neuron to the Renshaw cell. Under this assumption, these synapses have the same reversal potential, saturation voltage, and threshold voltage, but may differ in terms of maximum synaptic conductance. Resting potentials for the motor neurons, Ia inhibitory neurons, and Renshaw cells were set to -62 mV, -60 mV, and -50.5 mV, respectively [9,13,20]. Lastly, in the experiments done on cats during fictive locomotion, it was found that Ia neurons were most active in phase with the motor neurons, while the Renshaw cells became excited after motor neurons and were maximally excited in the latter phases of motor neuron excitement [14]. While this may not provide a quantifiable value for any of the neural parameters, it does indicate that the time constants for the motor neurons and Ia inhibitory neurons are similar while the Renshaw cells have a significantly larger time constant. Time constants for the model neurons are functions of the membrane capacitance and conductance: $\tau = C/G$. Based on the modeling in Animatlab, we give each neuron a conductance of one microsiemen and membrane capacitance's of 5, 30, and 130 nanofarads milliseconds for the motor neurons, Ia inhibitory neurons, and Renshaw cells, respectively [3]. After applying these assumptions and incorporating biological data, the number of parameters to be tuned was decreased from 72 to 37.

In order to properly evaluate the simulation as it compares to the animal data, we first needed to find a set of parameters which induces oscillations in the hip joint. As previously stated, this was done in a qualitative sense which primarily consisted of evaluating the outputs of the motor neurons for a give simulation. For example, Fig. 3 shows the results of a simulation whose parameter set does not result in oscillation of the hip joint. In the motor neuron plots in fig.

3 there is an initial phase of oscillatory behavior, however, this quickly dies out as the flexor motor neuron is not able to escape and overcome the extensor motor neuron. Based on these results the strengths of the synapses were adjusted to decrease the inhibition to the flexor motor neuron. This was done by decreasing the maximum synaptic conductance for the synapse coming from the extensor Ia inhibitory neuron to the flexor motor neuron.

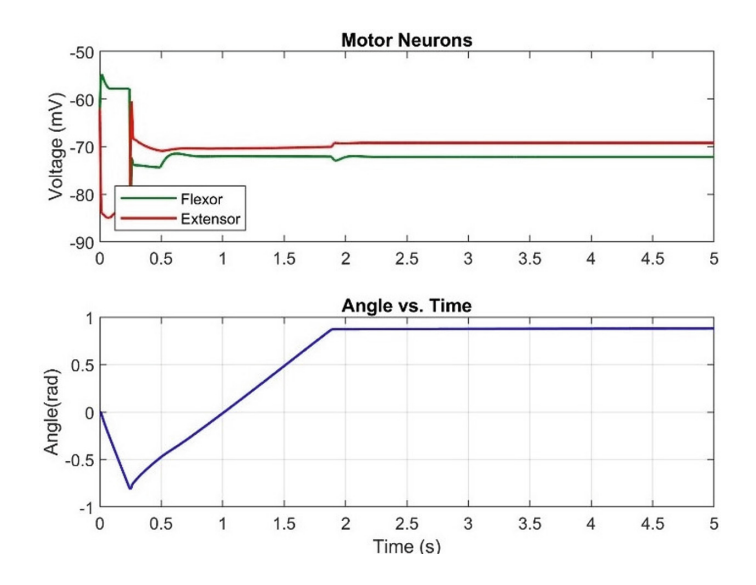


Fig. 3. Simulation results for a system with no oscillations. Top: Motor Neuron activity. Bottom: Hip joint activity.

Once a set of parameters was found which produced oscillatory behavior of the hip joint for the biomechanical model of the rat hindlimb, the tuning method switched to a quantitative analysis of the trajectory of the hip joint. This analysis was done by comparing the simulated hip joint vs. time to animal data. Note that the animal data is for the average hip trajectory of the rats during experiments, and may vary from step to step and animal to animal. The comparison was done in attempt to minimize a cost function, which was the sum of three equally weighted factors: the root means square error for a single stride, the frequency error, and the error in the swing/stance ratio. In the hip angle vs. time plots shown in Fig. 4, the stance and swing phases can be differentiated by the direction of motion. The stance phase corresponds to an increasing angle while the swing phase occurs while the angle is decreasing. The frequency and swing/stance ratio errors were taken in the form of percent error:

$$\%Error = \left| \frac{v_A - v_E}{v_E} \right| \tag{8}$$

where v_A is the observed value, in this case the simulated value, and v_E is the expected value, the value from the animal data. The values used for the simulated data were the averages over multiple gait cycles. Although this method was designed to provide a quantitative approach to the tuning of the CMM, the decisions on which parameters to change and how was largely based on knowledge gained during the tuning process.

3 Results

The CMM was successfully tuned such that the trajectory of the simulated hip joint matched the animal data. The oscillatory behavior is driven by the interplay between the fast Ia feedback from the muscles and the slow time constant of the Renshaw cells. Figure 4 shows the angle vs. time plots for the simulation and animal data for both a single and multiple gait cycles. The results from the simulation including neuron potentials and stretch receptor discharge rates can be found in Fig. 5. Note that the plot of the hip angle in Figs. 4 and 5 are the same data. Due to constraints in Animatlab, the joint angle begins at zero, Fig. 4 shows only the time period of oscillations, removing the initial descent into oscillatory behavior. The time axis was also shifted to remove this introductory period.

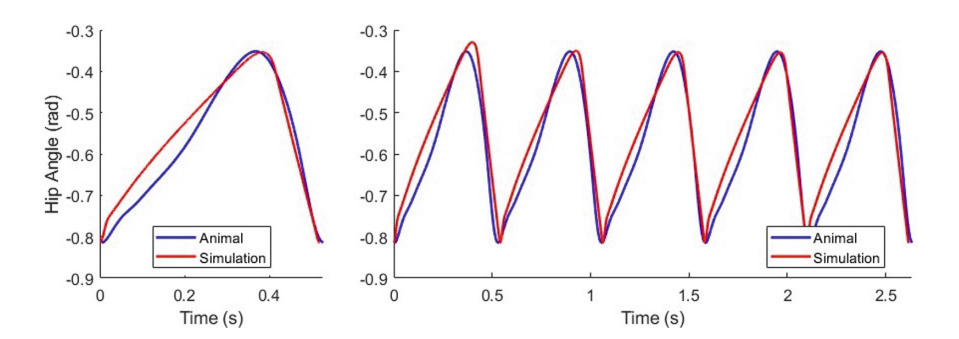


Fig. 4. Hip Angle vs. Time for simulated hindlimb and rat walking on a treadmill. Left: single gait cycle. Right: continuous oscillations. For the single gait cycle (left), transition from swing to stance occurs at 0.3582s seconds for the animal data and 0.3807s seconds for the simulated data.

The synaptic parameters in the simulation above can be found in Table 1. Notice that the strength of the synapse going from the extensor to the flexor Renshaw cell is zero. This indicates that, for this set of parameters, this synapse does not exist. Therefore, there is no reciprocal inhibition between the Renshaw cells. In addition to these synaptic parameters, the strength of the feedback from the stretch receptors had a significant impact on the behavior of the model. As shown in Eq. 2, this Ia type feedback is modeled as an applied current, Table 2 shows the values used to model this current. Table 2 also shows the amplification of the motor neuron output to the muscles.

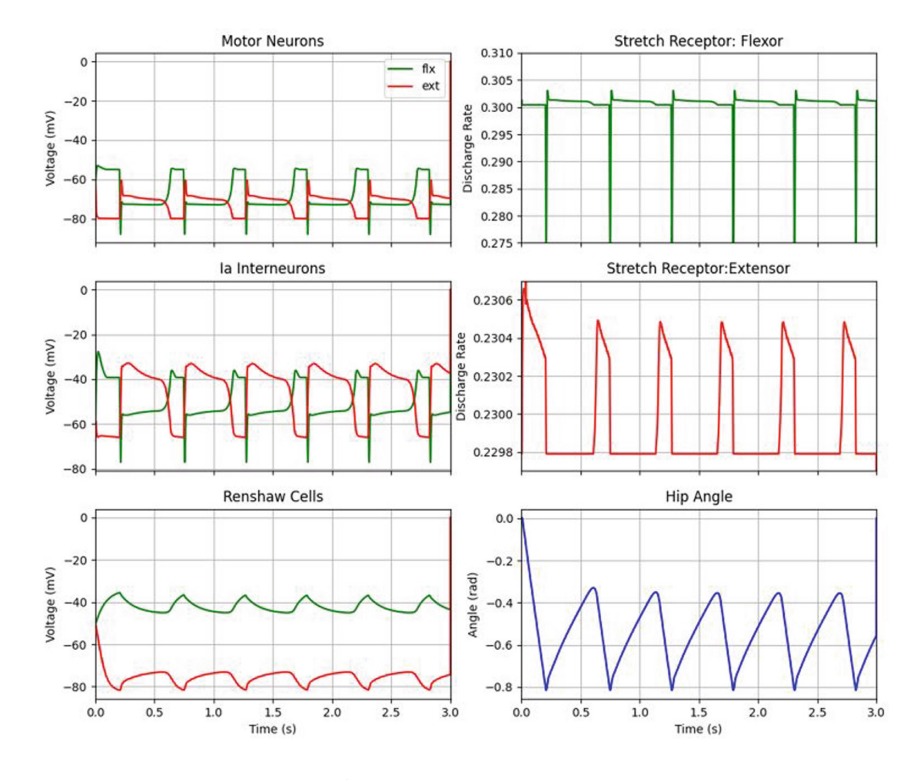


Fig. 5. Animatlab simulation outputs.

4 Discussion

The results show that a CMM modeled with non-spiking leaky-integrator neurons can be used to generate the oscillatory motion of a rat's hip joint which largely matches animal data. However, there is a noticeable difference in that the simulated hip angle rotates at relatively constant velocities for much of the stance and swing phases with a transition period between. Whereas the animal data shows a change in angular velocity throughout the stance and swing phases, as shown in Fig. 4. This is likely due to the simplified models of both the biomechanics and neural circuit in the simulation. For the given model, the hip joint is actuated by only two muscles forming an agonist-antagonist pair. In reality, the motion of a rat's hip joint is caused by the contraction of several muscles working together to cause a moment about the hip joint. The simplification to a single muscle lifting the leg vastly simplifies the forces acting on the joint. Additionally, each of the muscles in a rat may be activated by separate pools of motor neurons. The variation of motor neuron activity acting on different muscles would likely lead to a system with dynamics that more closely match the animal data. Although it is reasonable to assume that a more biologically accurate model would be able to fully capture the dynamics of the hip joint during locomotion, it is not a necessary step to evaluate the CMM. We also see

that the error in the hip trajectory is larger in the stance phase than in the swing phase. This is likely due to the simulation being done with an air stepping model and lacks the external forces from the treadmill acting on the body. The simplified models were able to replicate the trajectory of a rat's hip joint during locomotion well with understandable discrepancies.

Synapse (from - to)	g _{max} (μS)	E _{syn} (mV)	E _{hi} (mV)	E _{lo} (mV)
la flx. – la ext.	2.5	-99.7	-40	-62
la ext. – la flx.	2.198	-99.7	-40	-62
Ia flx. – MN ext.	1.076	-100	-40	-62
la ext. – MN flx.	1.0	-100	-40	-62
MN flx. – RC flx.	0.6	0	-54.35	-78
MN ext. – RC ext.	0.5	0	-54.35	-78
RC ext. – la ext.	5.0	-70	-40	-60
RC flx. – Ia flx.	4.2	-70	-40	-60
RC ext. – MN ext.	0.55	-70	-40	-60
RC flx. – MN flx.	0.45	-70	-40	-60
RC flx. – RC ext.	1.8	-100	-40	-60
RC ext. – RC flx.	0.0	-100	-40	-60

Table 1. Hand Tuned Synaptic parameters.

Relatively little work has been done to provide quantifiable values for the strength of the synapses in the CMM circuit. It had been predicted that the strength of inhibition acting on the motor neurons from the Renshaw cells was much less than the inhibition of the Ia neurons by the Renshaw cells. The resulting parameters shown in Table 1 support this claim as the strength of these synapses, represented by g_{max} , differ by an order of magnitude. Table 1 also shows that there is no mutual inhibition between Renshaw cells in this system. Therefore, the issue of the Renshaw cells as a point of gain control is unclear at present because the Renshaw cells have modest effects, but strong actions on the motor neurons [5]. This would indicate that the primary function of the Renshaw cells in this CMM model is to regulate the potential of the corresponding motor neurons.

Table 2. Hand Tuned Gain parameters (as used in Eq. 2). SR: Stretch Receptor. MN: Motor Neuron

Connection	Slope (m)	y-intercept (b)
SR – Ia Flx	10.032 μ	-2.864 μ
SR – la Ext	10.04 μ	-2.234 μ
SR – MN Flx	2.04 μ	-0.599 μ
SR – MN Ext	1.002 μ	-0.227 μ
MN – Flx Muscle	0.965	0
MN – Ext Muscle	1.026	0

While this is true for the set of parameters found in Table 1, this set of parameters is by no means the only set that would produce similar results. Therefore, it would be difficult to make any conclusions on the functionality of Renshaw cells with much certainty. It is reasonable to assume that there is a larger family of possible solutions for the various parameters in the model. The method of hand-tuning parameters failed to find these other solution sets. Ongoing work is being conducted to implement a Bayesian/Monte Carlo/Markov Chain approach that will automate the parameter search of the network [18]. Ideally this approach would search a larger space than was done through hand-tuning the network and would provide sets of parameters which produce similar results to those shown in Fig. 4 as opposed to the single set found while hand tuning. We could then compare the strength of the mutual inhibition between Renshaw cells for multiple sets of parameters to create a clearer image of their impact on motor output.

While the simulation has shown that a CMM is able to produce the rhythmic, oscillatory motion required for locomotion, it is likely that this circuit receives input from a central pattern generator [8,12,14,16]. However, this work aimed to evaluate the oscillatory properties of the isolated CMM. In future works, the CMM network will be evaluated with the addition of a CPG as an input to both the motor neurons and Ia inhibitory neurons. We can then compare the results of the CPG-fed CMM control strategy to previous works such as a two-layer CPG and muscle synergy and the functional subnetwork approach to neural controllers [4,6]. In this way we can evaluate various neural control strategies for robotics. Perhaps the more interesting implications of this research is the insight gained on the neural system. Through simulations such as this we can test theories in neuroscience and evaluate the purpose of specific neurons and synapses. This will ultimately lead to a better understanding of the neural circuitry responsible for locomotion in humans and animals alike and may inform medical efforts to restore motor function after spinal cord injuries.

References

- Alessandro, C., Rellinger, B.A., Barroso, F.O., Tresch, M.C.: Adaptation after vastus lateralis denervation in rats demonstrates neural regulation of joint stresses and strains. eLife 7, e38215 (2018). https://doi.org/10.7554/eLife.38215
- Charles, J.P., Cappellari, O., Spence, A.J., Wells, D.J., Hutchinson, J.R.: Muscle moment arms and sensitivity analysis of a mouse hindlimb musculoskeletal model. J. Anat. 229(4), 514–535 (2016). https://doi.org/10.1111/joa.12461
- Cofer, D., Cymbalyuk, G., Reid, J., Zhu, Y., Heitler, W.J., Edwards, D.H.: AnimatLab: a 3D graphics environment for neuromechanical simulations. J. Neurosci. Methods 187(2), 280–288 (2010). https://doi.org/10.1016/j.jneumeth.2010.01.005
- Deng, K., et al.: Neuromechanical model of rat hindlimb walking with two-layer CPGs. Biomimetics 4(1), 21 (2019). https://doi.org/10.3390/biomimetics4010021
- Hultborn, H., Lindström, S., Wigström, H.: On the function of recurrent inhibition in the spinal cord. Exp. Brain Res. 37(2), 399–403 (1979). https://doi.org/10.1007/ BF00237722
- Hunt, A., Szczecinski, N., Quinn, R.: Development and training of a neural controller for hind leg walking in a dog robot. Front. Neurorobot. 11, 18 (2017). https://doi.org/10.3389/fnbot.2017.00018
- Hunt, A.J., Szczecinski, N.S., Andrada, E., Fischer, M., Quinn, R.D.: Using animal data and neural dynamics to reverse engineer a neuromechanical Rat model. In: Wilson, S.P., Verschure, P.F.M.J., Mura, A., Prescott, T.J. (eds.) LIVING-MACHINES 2015. LNCS (LNAI), vol. 9222, pp. 211–222. Springer, Cham (2015). https://doi.org/10.1007/978-3-319-22979-9_21
- Ivashko, D., Prilutsky, B., Markin, S., Chapin, J., Rybak, I.: Modeling the spinal cord neural circuitry controlling cat hindlimb movement during locomotion. Neurocomputing 52–54, 621–629 (2003). https://doi.org/10.1016/S0925-2312(02)00832-9
- 9. Jiang, M., Heckman, C.: In vitro sacral cord preparation and motoneuron recording from adult mice. J. Neurosci. Methods **156**(1–2), 31–36 (2006). https://doi.org/10.1016/j.jneumeth.2006.02.002
- Johnson, W.L., Jindrich, D.L., Roy, R.R., Reggie Edgerton, V.: A three-dimensional model of the rat hindlimb: musculoskeletal geometry and muscle moment arms. J. Biomech. 41(3), 610–619 (2008). https://doi.org/10.1016/j.jbiomech.2007.10.004
- 11. MacKay-Lyons, M.: Central pattern generation of locomotion: a review of the evidence. Phys. Ther. 82(1), 69–83 (2002). https://doi.org/10.1093/ptj/82.1.69
- McCrea, D.A., Rybak, I.A.: Organization of mammalian locomotor rhythm and pattern generation. Brain Res. Rev. 57(1), 134–146 (2008). https://doi.org/10. 1016/j.brainresrev.2007.08.006
- 13. Perry, S., et al.: Firing properties of Renshaw cells defined by Chrna2 are modulated by hyperpolarizing and small conductance ion currents I $_{\rm handI_{sk}}$. Eur. J. Neurosci. 41(7), 889–900 (2015). https://doi.org/10.1111/ejn.12852
- Pratt, C.A., Jordan, L.M.: IA inhibitory interneurons and Renshaw cells as contributors to the spinal mechanisms of fictive locomotion. J. Neurophysiol. 57(1), 56–71 (1987). https://doi.org/10.1152/jn.1987.57.1.56
- Rubeo, S., Szczecinski, N., Quinn, R.: A synthetic nervous system controls a simulated cockroach. Appl. Sci. 8(1), 6 (2017). https://doi.org/10.3390/app8010006

- Rybak, I.A., Stecina, K., Shevtsova, N.A., McCrea, D.A.: Modelling spinal circuitry involved in locomotor pattern generation: insights from the effects of afferent stimulation: modelling afferent control of locomotor pattern generation. J. Physiol. 577(2), 641–658 (2006). https://doi.org/10.1113/jphysiol.2006.118711
- 17. Ramalinga setty, S.T., et al.: A whole-body musculoskeletal model of the mouse. IEEE Access $\bf 9,~163861-163881$ (2021). https://doi.org/10.1109/ACCESS.2021. 3133078
- Wang, Y.C., et al.: Algorithmic parameter estimation and uncertainty quantification for Hodgkin-Huxley neuron models. preprint, Neuroscience (2021). https:// doi.org/10.1101/2021.11.18.469189
- Wilson, H.R., Cowan, J.D.: Excitatory and inhibitory interactions in localized populations of model neurons. Biophys. J. 12(1), 1–24 (1972). https://doi.org/10.1016/S0006-3495(72)86068-5
- Wilson, J.M., Blagovechtchenski, E., Brownstone, R.M.: Genetically defined inhibitory neurons in the mouse spinal cord dorsal horn: a possible source of rhythmic inhibition of motoneurons during fictive locomotion. J. Neurosci. 30(3), 1137– 1148 (2010). https://doi.org/10.1523/JNEUROSCI.1401-09.2010